

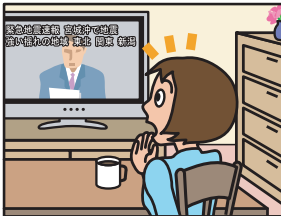
SEISMOLOGICAL RESEARCH LETTERS

Volume 80, Number 5

September/October 2009

At Home

- Protect your head and take shelter under a table
- Don't rush outside
- Don't worry about turning off the gas in the kitchen



In Public Buildings

- Follow the attendant's instructions
- Remain calm
- Don't rush to the exit



Earthquake Early Warning: Dos & Don'ts

When Driving

- Don't slow down suddenly
- Turn on your hazard lights to alert other drivers, then slow down smoothly
- If you are still moving when you feel the earthquake, pull over safely and stop



Remain calm, and secure your personal safety based on your surroundings!

After seeing or hearing an Earthquake Early Warning, you have only a matter of seconds before strong tremors arrive. This means you need to act quickly to protect yourself.

Outdoors



- Look out for collapsing concrete-block walls
- Be careful of falling signs and broken glass
- Take shelter in a sturdy building if there is one close enough

On Buses or Trains

Hold on tight to a strap or a handrail



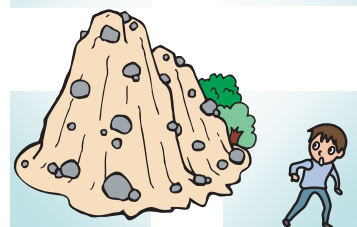
In Elevators

Stop the elevator at the nearest floor and get off immediately



Near Mountains/Cliffs

Watch out for rockfalls and landslides



Testing ElarmS in Japan

Holly M. Brown and Richard M. Allen

Seismological Laboratory, University of California, Berkeley

Veronica F. Grasso

Group on Earth Observations, Geneva, Switzerland

INTRODUCTION

Earthquake early warning systems use seismic networks, rapid telemetry, and software algorithms to detect an earthquake immediately after its inception, estimate its damage potential, and disseminate a warning to surrounding communities before peak ground shaking occurs. Earthquake Alarm Systems, or ElarmS, is an earthquake early warning system developed in California. The ElarmS algorithm recognizes earthquakes from the initial *P*-wave arrivals at seismometers near the epicenter. The characteristics of the *P* wave, including amplitude and frequency, are used to estimate a final magnitude for the event. *P*-wave arrival times from several stations are combined to estimate the hypocenter of the event. Finally, the estimated magnitude and hypocenter are applied to attenuation relations to produce a prediction of ground shaking levels in the region.

ElarmS has been tested extensively with datasets of earthquakes from northern and southern California (Allen and Kanamori 2003; Allen 2007; Wurman *et al.* 2007; Tsang *et al.* 2007; Allen *et al.* 2009). While the test datasets from California included a large range of locations and source types, there are a limited number of recent, well-recorded, large earthquakes available for testing the early warning system. In this study we take ElarmS to another geographic and seismic setting and test the algorithms with a dataset of 84 large-magnitude earthquakes, including 43 of magnitude 6.0 or greater, in Japan. The Japanese test dataset is valuable both for the insight into ElarmS' processing of large events and for the chance to process events in a completely different geologic setting. The offshore and deep nature of many of the events presents new challenges to the methodology. The Japanese earthquakes offer an opportunity to improve the robustness of ElarmS, extend its abilities to other settings, and confirm its relevance for large-magnitude events.

EARTHQUAKES DATASET

The dataset contains 84 earthquakes recorded by Japan's Kyoshin Net (K-NET) strong-motion seismic network. K-NET consists of 1,000 digital strong-motion seismometers, distributed across Japan with approximately 25-km spacing. Each station is capable of recording accelerations up to 2,000 cm/s²,

with a sampling frequency of 100 samples per second and a dynamic range of 100 dB.

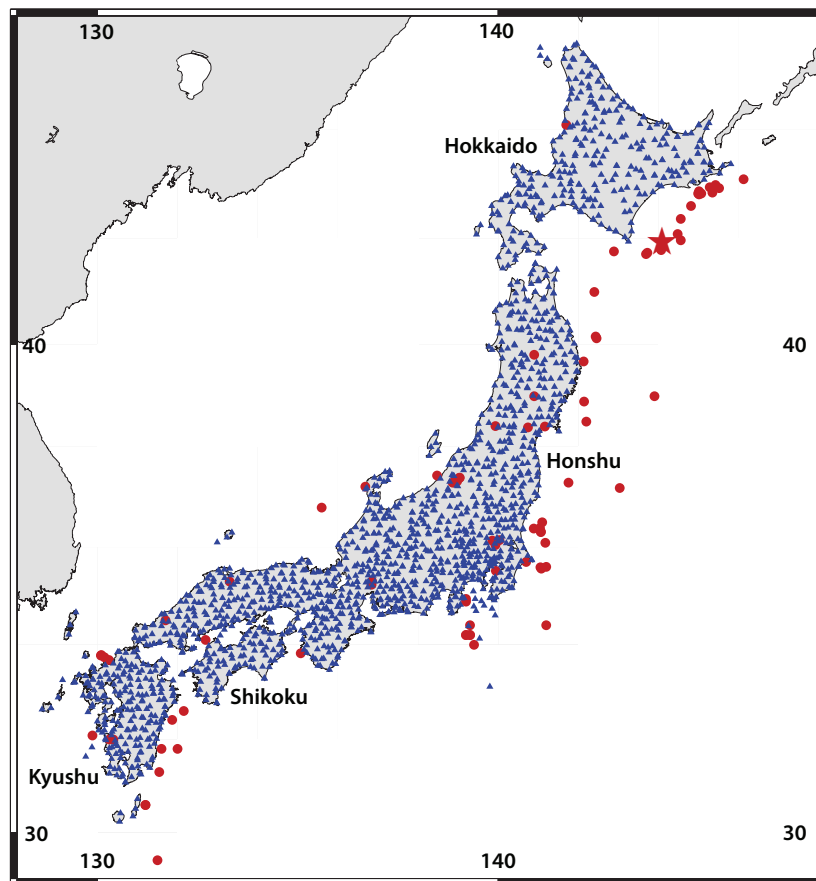
The 84 test earthquakes occurred between September 1996 and June 2008 (Figure 1). The waveforms were downloaded directly from the K-NET website (<http://www.k-net.bosai.go.jp>). All events occurred within 100-km hypocentral distance of at least three stations. The Japan Meteorological Society (JMA) magnitude estimates range from 4.0 to 8.0. Forty-three events have magnitudes of 6.0 or greater. The largest event in the dataset is the Tokachi-Oki earthquake of 26 September 2003, which had a magnitude of 8.0.

WARNING METHODOLOGY

Location

When only one station has triggered on a *P*-wave arrival, ElarmS sets the estimated hypocenter directly beneath the station, at a depth of 8 km. When a second station triggers, or if the first two stations trigger simultaneously, ElarmS locates the event on the great circle between the two stations, at a location dependent on their arrival times, again at a fixed depth of 8 km. When three stations have triggered, ElarmS triangulates an event epicenter using a two-dimensional grid search, the arrival times at each of the stations, and a typical *P*-wave velocity. The depth is still fixed at 8 km.

In California, this third method continues to be used when four, five, or more stations have triggered. The use of a two-dimensional grid search and fixed depth are acceptable for the shallow seismogenic zone in most of California. In the Japanese subduction zone, however, this is inappropriate. For the Japanese dataset a three-dimensional location algorithm is needed. The first three scenarios, for one, two, or three triggers, remain the same. When four or more stations have triggered, ElarmS creates a three-dimensional grid of possible event hypocenters, with depths ranging from 0 km to 100 km in steps of 10 km. Observed *P*-wave travel times are compared to those predicted by travel time curves for seismic waves originating at each point of the grid. The best match of arrival times is deemed to be the event hypocenter. As additional stations trigger, the grid search is repeated and the estimated hypocenter is updated.



▲ **Figure 1.** Location map. Red circles are events used in this study, blue triangles are K-NET stations. The red star is the largest event in our dataset, the **M 8.0 Tokachi-Oki earthquake of 2003.**

Magnitude

ElarmS uses two P -wave parameters, peak amplitude and maximum predominant period, to create two independent estimates of final event magnitude. The estimates from each parameter are then averaged together to form the ElarmS magnitude for the event.

Maximum predominant period, τ_p^{\max} , was developed first and provided the original framework for ElarmS (Allen and Kanamori 2003). For a given region, observed τ_p^{\max} values from the first few seconds of the P wave are plotted as a function of final event magnitude. A least-squares fit to the data results in τ_p^{\max} vs. magnitude scaling relations for the region (Allen and Kanamori 2003; Lockman and Allen 2005; Wurman *et al.*, 2007; Tsang *et al.* 2007). These empirically determined scaling relations are then used to estimate magnitude.

For a given event, the first station to recognize a P -wave arrival reports a τ_p^{\max} value after one second of observation. As additional seconds pass, the station may update that value if a larger τ_p^{\max} is observed. When more stations trigger, they too initially report one-second τ_p^{\max} values, which may increase with additional seconds of data. Each second, ElarmS applies the scaling relations to the most current τ_p^{\max} observation from each triggering station to determine an estimated magnitude. All station magnitudes are then averaged together to create a single τ_p^{\max} -based magnitude. This averaged magnitude esti-

mate is adjusted every second, as current stations update their τ_p^{\max} observations and new stations trigger.

Peak displacement amplitude, P_d , of the P wave was added as an ElarmS parameter by Wurman *et al.* in 2007. For a given region, observed P_d values are recorded at each station, scaled to a common epicentral distance, and plotted against final event magnitude. Again, a least-squares fit is used to determine regional P_d vs. magnitude scaling relations. During event processing, P_d observations are combined in the same way as τ_p^{\max} observations. Each triggered station reports a P_d observation every second. The P_d value may increase if a large displacement is observed later in the P wave. ElarmS converts each P_d observation to an estimated magnitude and then averages all the estimated magnitudes together to create a single P_d -based magnitude. As more P_d observations become available, they are incorporated into the estimate.

ElarmS performs each of these scaling calculations independently, resulting in one τ_p^{\max} -based magnitude estimate and one P_d -based magnitude estimate each second. The two magnitudes are averaged together to create the ElarmS magnitude estimate, which is used for predicting ground shaking. ElarmS uses a simple linear average of the two methods, as we have yet to observe an improvement with the use of a weighted average (Wurman *et al.* 2007).

AlertMaps

Once a hypocenter and magnitude are estimated, ElarmS predicts regional ground accelerations from attenuation relations. For Japan, ElarmS uses the same attenuation relations that the National Earthquake Information Center (NEIC) uses to create ShakeMaps for Japanese events (Wald *et al.* 2005). For events shallower than 20 km or with magnitude less than 7.7, the attenuation relations are those defined by Boore *et al.* (1997). For all other events in Japan, the attenuation relations are those from Youngs *et al.* (1997).

The initial AlertMap is generated using only the estimated magnitude and event location. As stations begin observing peak ground acceleration (PGA), the observations are incorporated into the AlertMap and the attenuation function is adjusted to best fit the available data. The intent of including PGA observations is to correct for any errors in the ElarmS estimate of magnitude. As each PGA observation is added, the AlertMap predictions are adjusted closer to the true observed ground motions. If the catalog magnitude and location are used for an event, and all PGA observations are included, then by definition the AlertMap exactly equals the U.S. Geological Survey (USGS) ShakeMap for that event. Using the estimated magnitude and location, any error in the final AlertMap after all PGA observations are included is thus due to errors in the magnitude and location estimates.

Error Calculations

Errors are calculated by comparing ElarmS' output to published or observed values. For magnitude and location, the ElarmS estimate is compared to the K-NET published magnitude and location. For ground motions, the ElarmS prediction for any station that has not yet observed peak ground shaking is compared to the final observation at that station. Only predictions that are made before peak ground shaking occurs are considered for the error analysis.

SYSTEM PERFORMANCE

Magnitude Estimation

We begin by determining the scaling relationship between peak displacement (P_d) and magnitude in Japan. Acceleration data from each station is double-integrated to displacement and scaled to a common epicentral distance of 10 km. These scaled displacements are then plotted as a function of the K-NET catalog magnitude (M_L). Applying a least-squares fit to the observed $\log_{10}(P_d)$ values gives a scaling relation of $\log_{10}(P_d) = 0.66 * M_L - 4.02$, shown in Figure 2(A). The dashed line in the figure is the scaling relation for northern California, $\log_{10}(P_d) = 0.73 * M_w - 3.77$ (Wurman *et al.* 2007). The scaling relation for Japan is of a similar slope to that of northern California, but with lower displacements at all magnitudes. This implies that Japan has higher attenuation than northern California.

P_d observations from all events are weighted equally in the determination of the P_d scaling relations. We note that the largest event, the M 8.0 Tokachi-Oki earthquake, does not fall

on the scaling relations. Using the observed displacements for Tokachi-Oki and the P_d scaling relations determined from all events, ElarmS underestimates the event magnitude by more than one magnitude unit. Other studies have shown that peak displacements may saturate at near-source stations during large magnitude events (Wurman *et al.* 2007; Zollo *et al.* 2006). This is the effect we observe for the largest earthquake in our dataset. The relatively low amplitudes near the source can lead to underestimation of magnitude. This suggests that P_d should not be used alone in regions that are prone to very large earthquakes.

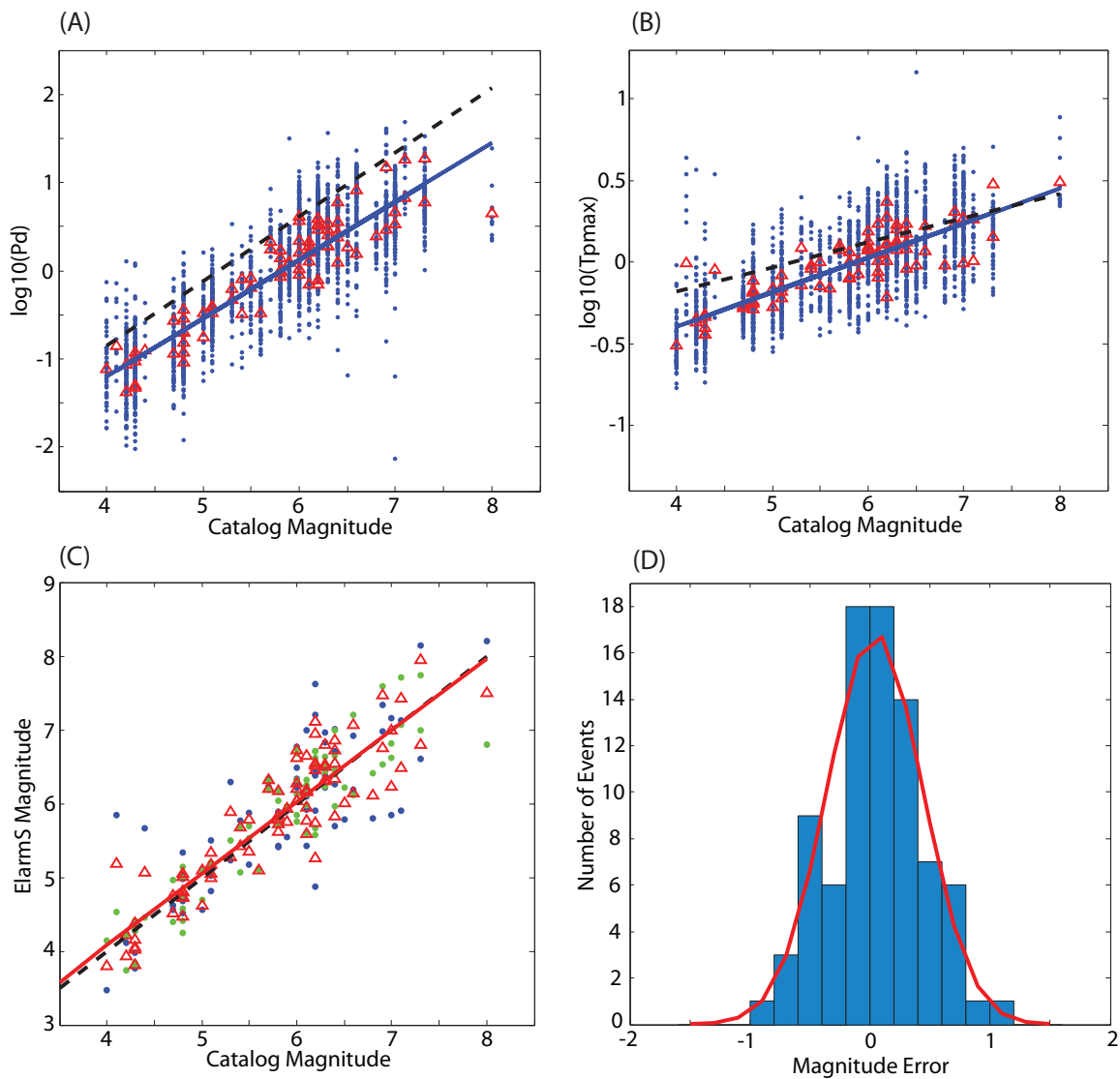
The second magnitude estimation method is maximum predominant period, or τ_p^{\max} . The observed τ_p^{\max} values at each station are plotted in Figure 2(B) against the final catalog magnitude of each event. A least-squares fit to the data produces a scaling relation of $\log_{10}(\tau_p^{\max}) = 0.21 * M_L - 1.22$, shown as the solid line in Figure 2(B). Wurman *et al.* (2007) found a scaling relation for northern California of $\log_{10}(\tau_p^{\max}) = 0.15 * M_w - 0.78$, shown as the dashed line. The observed predominant periods in Japan are of similar values to those of northern California, but the best-fit slope is steeper in Japan. τ_p^{\max} does not appear to display the saturation effects that P_d does. For the M 8.0 Tokachi-Oki event, using the best fit scaling relation and τ_p^{\max} observations leads to an estimated magnitude of 8.2, using τ_p^{\max} alone. However, τ_p^{\max} shows more scatter than P_d , particularly for the lowest magnitude events. This agrees with similar results found by previous studies (Olson and Allen 2005; Wurman *et al.* 2007).

ElarmS produces a single event magnitude by averaging together the magnitudes from P_d and τ_p^{\max} . Figure 2(C) shows the three magnitude estimates for each event. The green points are the magnitude estimates for each event using only P_d observations at each station. The blue points are the magnitude estimates using only τ_p^{\max} , and the red points are the final magnitude estimate for each event when τ_p^{\max} and P_d magnitudes have been averaged together. The red line is the linear best fit to the averaged magnitudes. The dashed black line is the desired 1-1 fit, for which the ElarmS estimated magnitude would be exactly equal to the K-NET catalog magnitude. The averaged magnitudes fall close to the desired 1-1 fit, improving on both the saturation effects of P_d at high magnitudes and the scatter of τ_p^{\max} at low magnitudes. For the M 8.0 event, the averaged ElarmS magnitude is 7.5, one half unit lower than the published magnitude.

Figure 2(D) shows a histogram of the error in the average magnitude estimates from Figure 2(C). The red curve in the figure is the best-fit Gaussian distribution. The mean error is 0.0, with a standard deviation of 0.4 magnitude units. All but one event is within one magnitude unit. The one deviant event is a magnitude 4.1. The τ_p^{\max} observations for that event are high, leading to an average magnitude of 5.18.

Magnitude Estimation of Largest Events

Of primary concern is the accuracy of ElarmS' magnitude estimates for large-magnitude events. We consider subsets of the dataset, analyzing events within specific magnitude ranges.



▲ **Figure 2.** Scaling Relations. (A) Scaling relations for peak displacement. Blue circles are $\log_{10}(P_d)$ values observed at individual stations and corrected for distance. Red triangles are average peak displacements for each event. Solid blue line is the linear best fit to this data, $\log_{10}(P_d) = 0.66 \times M_L - 4.02$. Dashed black line is the linear best fit for northern California, $\log_{10}(P_d) = 0.73 \times M_w - 3.77$ (Wurman *et al.* 2007). (B) Scaling relations for maximum predominant period. Blue circles are $\log_{10}(\tau_p^{max})$ values observed at individual stations. Red triangles are average τ_p^{max} for each event. Solid blue line is linear best fit to this data, $\log_{10}(\tau_p^{max}) = 0.21 * M_L - 1.22$. Dashed black line is linear best fit for northern California, $\log_{10}(\tau_p^{max}) = 0.15 * M_w - 0.78$ (Wurman *et al.* 2007). (C) ElarmS magnitude for each event. The green circles are magnitudes using only P_d , the blue circles are magnitudes using only τ_p^{max} , and each red triangle is the average of the P_d and τ_p^{max} magnitudes for that event. The solid red line is the linear best fit to the average magnitudes (red triangles). The black dashed line is the ideal 1-1 fit, for which every ElarmS magnitude exactly equals the catalog magnitude for that event. (D) The histogram of errors in the average ElarmS magnitude estimates from (C). The red line is the best-fit Gaussian distribution for the magnitude errors and has a mean of 0.0 and standard deviation of 0.4.

For events with magnitude 6 or greater, the mean error is 0.04 magnitude units, with a standard deviation of 0.46. This is only slightly higher than the mean and standard deviation for all events. For events of magnitude 7 or greater (of which there are eight in this dataset, including the M 8.0 Tokachi-Oki event), the ElarmS magnitude has a mean error of -0.21, with a standard deviation of 0.53. This underestimation for the largest events is partly due to the saturation of P -wave amplitudes for large events but is also related to the offshore location of the

largest events. Poor azimuthal coverage causes large errors in the estimated epicentral distance, which in turn contaminates the magnitude determined by peak displacement.

Magnitude Dependence on Time

Each station reports to ElarmS once every second, updating its observed values of displacement and period. The peak displacement may occur in the first second after a trigger, or it may occur later. If a larger displacement is observed in later seconds, the

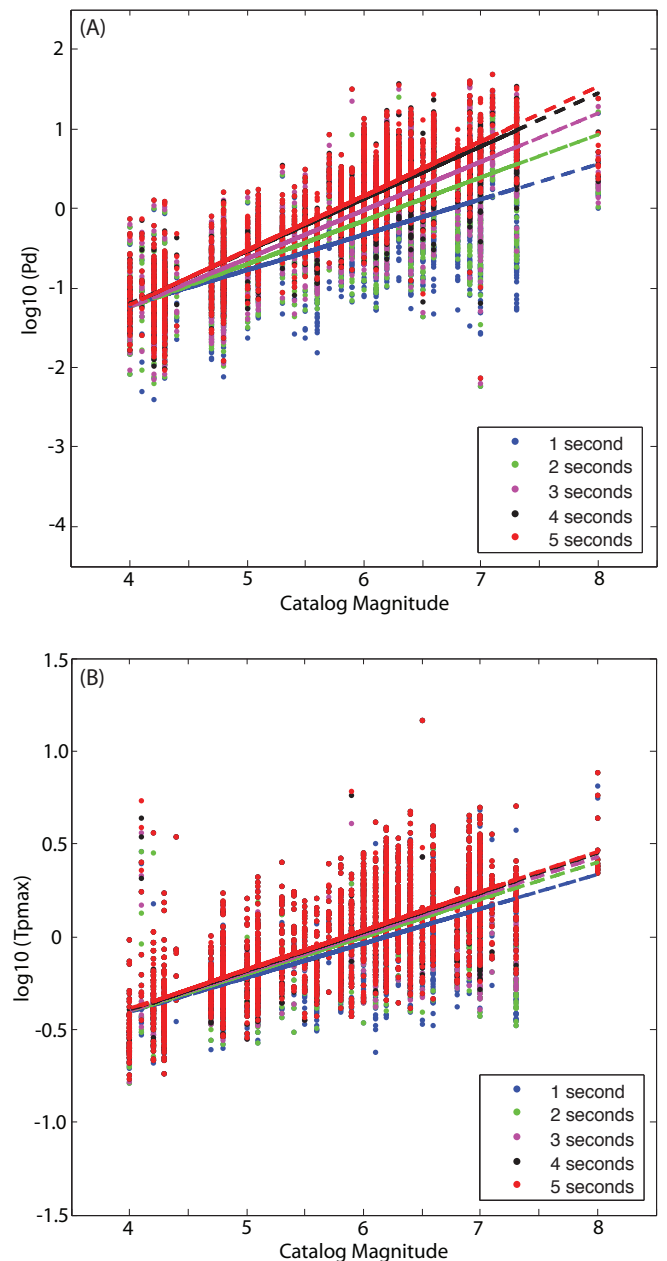
peak value for that station will be increased accordingly. If the one-second value continues to be the largest as additional seconds of data are recorded, that one-second peak is kept throughout. Thus the peak displacement recorded in the first second is the minimum possible value for that station. The same is true for maximum predominant period, τ_p^{\max} . The one-second observation of τ_p^{\max} is the minimum value for that station. It may be increased with additional seconds of data, but not decreased.

Magnitude error is thus directly dependent on the number of seconds of data available at each station. In Figure 3 we calculate separate scaling relations for each time window. Figure 3(A) shows the resulting scaling relations for peak displacement, P_d , given a one-, two-, three-, four-, or five-second window. Using one second of data at each station results in a shallow slope to the scaling relation, leading to systematic underestimation of magnitude for larger events. Each additional second of data increases the slope and improves the magnitude estimate for large events. The change from four to five seconds is minimal. We therefore determine that four seconds is the optimal time window, providing the most data while still allowing rapid response to the earthquake.

Figure 3(B) shows the effect of time window on maximum predominant period. τ_p^{\max} is less sensitive to time window but still shows a slight increase in slope and improvement in magnitude estimate with additional seconds of data. The fit to large events in particular improves with additional seconds. This verifies the finding of Allen and Kanamori (2003) that the initial magnitude using one second of data is a minimum estimate, and additional seconds of data increase the magnitude estimate for large events. Again the four-second window maximizes data availability and timeliness.

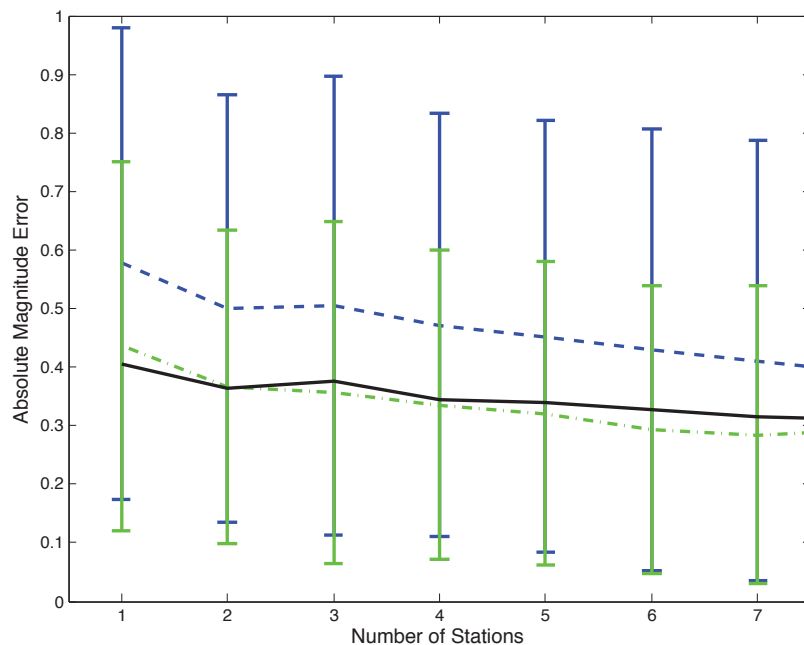
Magnitude Dependence on Stations

Any earthquake early warning system is dependent on data that arrives one station at a time. We test the sensitivity of the scaling relations to the number of stations reporting triggers. The stations are sorted by distance to the epicenter, and only the closest one, two, three, etc., stations are used to estimate magnitude. Figure 4 shows the absolute value of error in ElarmS magnitude estimates as additional station data is incorporated. The green and blue dashed lines are the error in the independent magnitude estimates made using only P_d or τ_p^{\max} , respectively. The solid line is the error in the averaged magnitude estimate, which ElarmS uses to predict ground motions in the region. This combined P_d and τ_p^{\max} estimate has an average absolute error of less than 0.42 magnitude units using only the single closest station to the epicenter, and the error decreases with the addition of more stations. P_d by itself produces an average error of less than half a magnitude unit for all numbers of stations. τ_p^{\max} by itself has higher error values than P_d , but still less than 0.6 magnitude units on average. Using only the closest one or two stations to the epicenter, the average error (solid line) is lower than both individual errors. This is because one method may overestimate the magnitude and the other may underestimate it; their average is closest to the true magnitude. Once three or more stations are providing data the average error in



▲ **Figure 3.** Effect of number of seconds of P -wave data on scaling relations. Circles are observations at individual stations, and lines are linear best-fit scaling relations to circles of the same color. Blue circles are observations made using only one second of P -wave data at each station; blue line is linear best-fit scaling relation using only one second of data. Green is two seconds of data, purple is three seconds, black is four seconds, and red is five seconds. (A) Effect of number of seconds of P -wave data on peak displacement (P_d) scaling relations. (B) Effect of number of seconds of P -wave data on maximum predominant period (τ_p^{\max}) scaling relations.

the magnitude using P_d alone is slightly lower than the average estimate. However, given the uncertainties (error bars in Figure 4) this difference is insignificant and we prefer to use two independent magnitude estimates rather than relying on just one.



▲ **Figure 4.** Effect of number of stations on the accuracy of magnitude estimates. The blue dashed line is the average error in magnitude estimates made using only maximum predominant period, τ_p^{\max} . The green dashed line is the average magnitude error using only peak displacement, P_d . The solid black line is the error when the two estimates are averaged.

Magnitude Error Distributions

Every ElarmS magnitude estimate is dependent on both the number of seconds of data at each station and the number of stations reporting. If we wish to know the uncertainty in a given magnitude estimate, we must consider the quantity of data included in the estimate. Figure 5 shows magnitude error histograms and best-fit Gaussian probability distributions, determined for specific quantities of data. The mean and standard deviation for all the error distributions are shown in Table 1. Figures 5(A) and (B) use exactly one second of P -wave arrival at each station. Figure 5(A) shows the error histogram when the closest five stations each contribute one second of data. The curves in Figure 5(B) represent the best-fit Gaussian error distributions when one, two, three, four, or five stations each contribute one second of data to the magnitude estimate. Figures 5(C) and (D) are for two seconds of data, Figures 5(E) and (F) for three seconds, and so on up to five seconds of data in Figures 5(I) and (J). The probability distributions get more peaked in each row, indicating that additional seconds of data improve the accuracy of the magnitude estimate.

More data for a magnitude estimate is always desirable, but an early warning system must be prompt to be useful. ElarmS creates its initial magnitude estimate using the first second of data at the first triggered station and then updates the estimate as more data becomes available. The error distributions shown in Figure 5 can be used to assign an uncertainty to the ElarmS magnitude estimate from the first estimate when one second of data is available.

Location

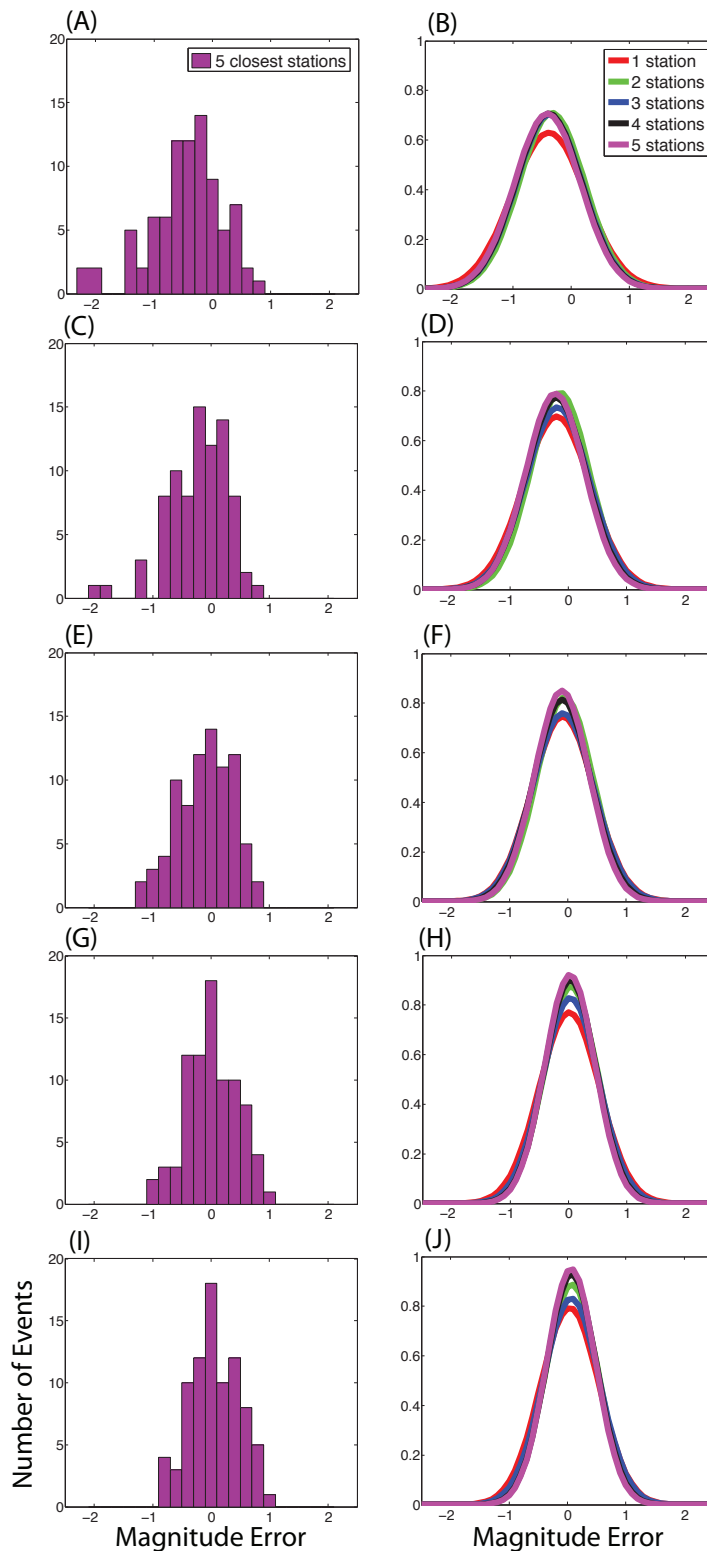
The Japanese events presented a challenge in that many occurred offshore (Figure 1). The ElarmS location algorithm depends on

triangulating between several stations, but this can be hindered by poor azimuthal coverage. For many events all stations are to the west, and the process of locating the hypocenter accurately requires more stations than it does for onshore events. Many events are also very deep, and a minimum of four stations must be available before hypocentral depth can be estimated. The mean error in the hypocentral location for all events and any number of stations providing arrival times, *i.e.*, one station up to the total number of triggering stations for each event, is 18 kilometers. The greatest errors are for those events occurring farthest offshore or deepest. Figure 6(A) shows a histogram of hypocentral location errors, using P -wave arrival times from five stations. The errors using one to five stations are listed in Table 1. We determine the best-fitting log-normal distributions (Figure 6B) for location error. These distributions can be used to estimate the error in any given ElarmS location, as a function of the number of stations reporting triggers.

Attenuation Relations

The final source of error is the attenuation relation used to translate magnitude and location into a prediction of local ground acceleration. To isolate this error we give ElarmS the catalog magnitude and location for each event. ElarmS applies those parameters to the ShakeMap attenuation relations for Japan to create an initial AlertMap prediction of ground motions. As stations report peak ground shaking observations, ElarmS incorporates them into the model and adjusts the predictions accordingly. Thus the only sources of error in the final PGA predictions are the attenuation calculations themselves, and any scatter in the local PGA observations.

The predictions are then compared to the actual observed ground motions recorded at any station whose data is not yet



▲ **Figure 5.** Error histograms for magnitude and corresponding probability distributions showing the effects of the number of stations and number of seconds of data. Each row contains one sample histogram and five probability distributions for one, two, three, four, and five stations providing a specific number of seconds of *P*-wave data. The colors within each row indicate the number of stations used. Red is one station, green is two stations, blue is three stations, black is four stations, and purple is five stations. (A) Magnitude error when the first one second of *P*-wave arrival is used from the closest five stations. (B) Error distributions using one to five stations, all with one second of *P*-wave data each. (C, D) Error using the first two seconds of *P*-wave data at each station. (E, F) Error using the first three seconds. (G, H) Error using the first four seconds. (I, J) Error using the first five seconds.

TABLE 1
Mean ± Standard Deviation of Error Distributions Used by Error Model

	0 stations	1 station	2 stations	3 stations	4 stations	5 stations
Mag, 1 sec	—	-0.38 ± 0.63	-0.33 ± 0.56	-0.37 ± 0.57	-0.39 ± 0.56	-0.41 ± 0.56
Mag, 2 sec	—	-0.2 ± 0.57	-0.15 ± 0.5	-0.18 ± 0.54	-0.21 ± 0.52	-0.22 ± 0.50
Mag, 3 sec	—	-0.09 ± 0.53	-0.05 ± 0.48	-0.08 ± 0.52	-0.10 ± 0.49	-0.10 ± 0.47
Mag, 4 sec	—	0.01 ± 0.52	0.04 ± 0.46	0.03 ± 0.48	0.03 ± 0.44	0.02 ± 0.43
Mag, 5 sec	—	0.04 ± 0.50	0.07 ± 0.45	0.07 ± 0.48	0.07 ± 0.43	0.06 ± 0.42
Location	—	33.6 ± 17.9	32.1 ± 21.4	32.5 ± 18.7	18.8 ± 13.6	21.1 ± 16.8
PGA	0.11 ± 0.30	0.09 ± 0.35	0.08 ± 0.37	0.06 ± 0.29	0.10 ± 0.28	0.03 ± 0.30

incorporated into the model. Figure 7(A) shows a histogram of the resulting errors when five PGA observations are included. Table 1 lists the mean errors using zero to five PGA observations. Figure 7(B) shows the probability distributions derived from the error data. The yellow curve is the initial ground-motion estimates, using only magnitude and location with no peak shaking observations. As stations report peak ground shaking, their observations are used to adjust the AlertMap PGA predictions up or down. The remaining curves show the error in the adjusted PGA predictions when actual PGA observations are included. Using one or two PGA observations results in the most error, more than the zero-observations case. The increased error using only one or two PGA observations occurs because each peak ground acceleration observation is affected by unpredictable path effects and may have significant variability compared to the average regional ground shaking. Only after several individual station observations are included do their individual errors cancel each other out. The errors using three, four, or five PGA observations are better than those of the zero-observation case. This suggests ElarmS should use the initial, zero-observation model until at least three PGA observations are available.

Example Earthquake

Figure 8 shows a step-by-step progression of ElarmS processing for an example event in Japan. The event is a magnitude 6.4, occurring 26 July 2003, at a depth of 11.9 km. The first two triggers are recognized at two stations simultaneously (Figure 8A). ElarmS places the event location between the two stations at a fixed depth of 8 km. One second later (Figure 8B), ElarmS combines the P_d and τ_p^{\max} observations from these two stations to create a magnitude estimate of 6.6 and predicts the distribution of ground shaking. A third station triggers, and the epicenter is estimated, with depth still fixed at 8 km. One second later (Figure 8C), which is two seconds after the first trigger, the third station's data is incorporated into the estimate, and magnitude is decreased to 6.2. Two more stations trigger, and the five total triggers so far are used to estimate a hypocenter, at a depth of 10 km. Finally, Figure 8(D) shows the ElarmS AlertMap when all data for the event are available, 12 seconds after the first trigger. The final ElarmS magnitude estimate is **M** 6.4. The magnitudes include P_d and τ_p^{\max} observations from

all 26 available stations, and the AlertMap is adjusted for peak ground shaking observations from all 26 stations.

ElarmS ERRORS

The Error Model

To determine the total error in the ElarmS prediction of ground shaking, we combine the errors determined for magnitude, location, and attenuation relations. The mean and standard deviation from each probability distribution above are used to run a Monte Carlo simulation, generating random errors within each distribution. These errors are then factored into the ground motion predictions using the NEIC's preferred attenuation relations for Japan. The NEIC global attenuation relations use either the Boore *et al.* (1997) or the Youngs *et al.* (1997) model, depending on depth and magnitude of the event. ElarmS follows the same criteria, choosing between the two models accordingly. For the example below, we show the error calculations from Boore *et al.* (1997). The coefficients (B_1, B_2, B_3, B_5) are those recommended by Boore for a reverse mechanism event.

The "expected" ground motions are determined by applying the catalog magnitude and location to the attenuation relations with no errors. This represents the ideal output from ElarmS, if all estimates were perfect.

Ideal output:

$$\ln(\text{PGA})_{\text{ideal}} = B_1 + B_2 \times (M - 6) + B_3 \times (M - 7) + B_5 \times \ln(R)$$

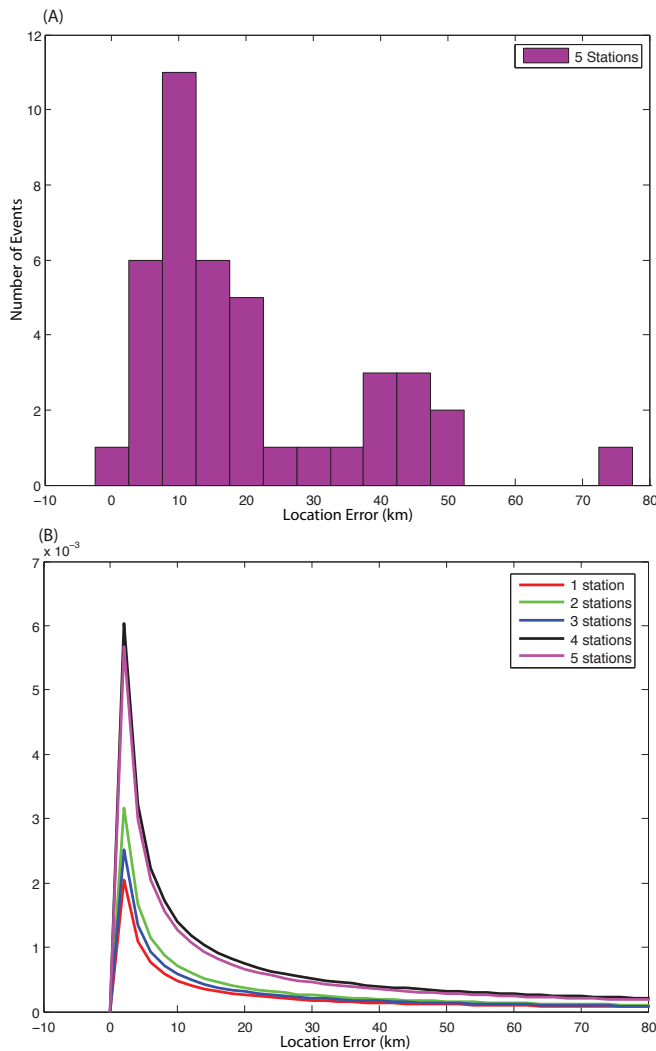
M is the magnitude, R is the distance from the event epicenter to the location whose PGA is being predicted, and $B_1, B_2, B_3,$ and B_5 are coefficients.

To calculate the ground-motion estimates provided by ElarmS, the catalog magnitude and location are again applied to the attenuation relations, but now with the addition of the errors generated by the Monte Carlo simulation.

Estimated output:

$$\ln(\hat{\text{PGA}}) = B_1 + B_2 \times (M + \varepsilon_M - 6) + B_3 \times (M + \varepsilon_M - 7) - B_5 \times \ln(R \pm \varepsilon_R) + \varepsilon_{\text{Att}}$$

The total error in the ElarmS estimated ground motions is the difference between the ideal and estimated values.

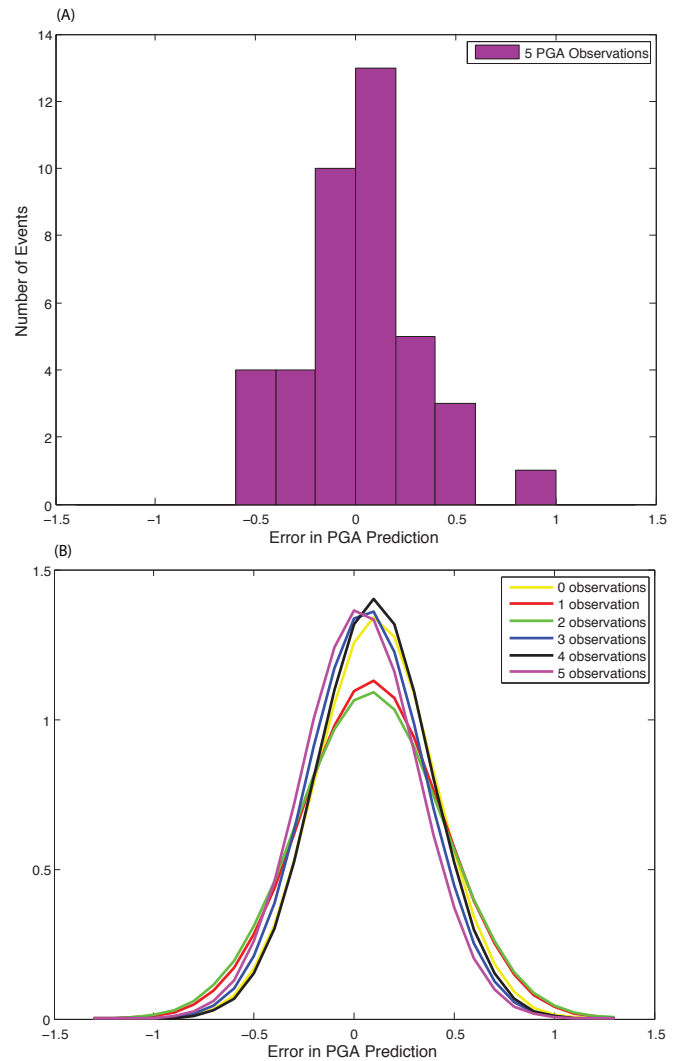


▲ **Figure 6.** (A) Histogram of error in location estimate when five stations provide P -wave arrival times. (B) Best-fit log-normal distributions to location errors as a function of the number of stations providing trigger times. Red is error in location estimates when only one station trigger is used to estimate event location. Green is error when two stations are used. Blue uses three stations, black uses four stations, and purple uses five stations.

$$\text{Error: } \varepsilon_{\text{PGA}} = \ln(\text{PGA})_{\text{ideal}} - \ln(\hat{\text{PGA}})$$

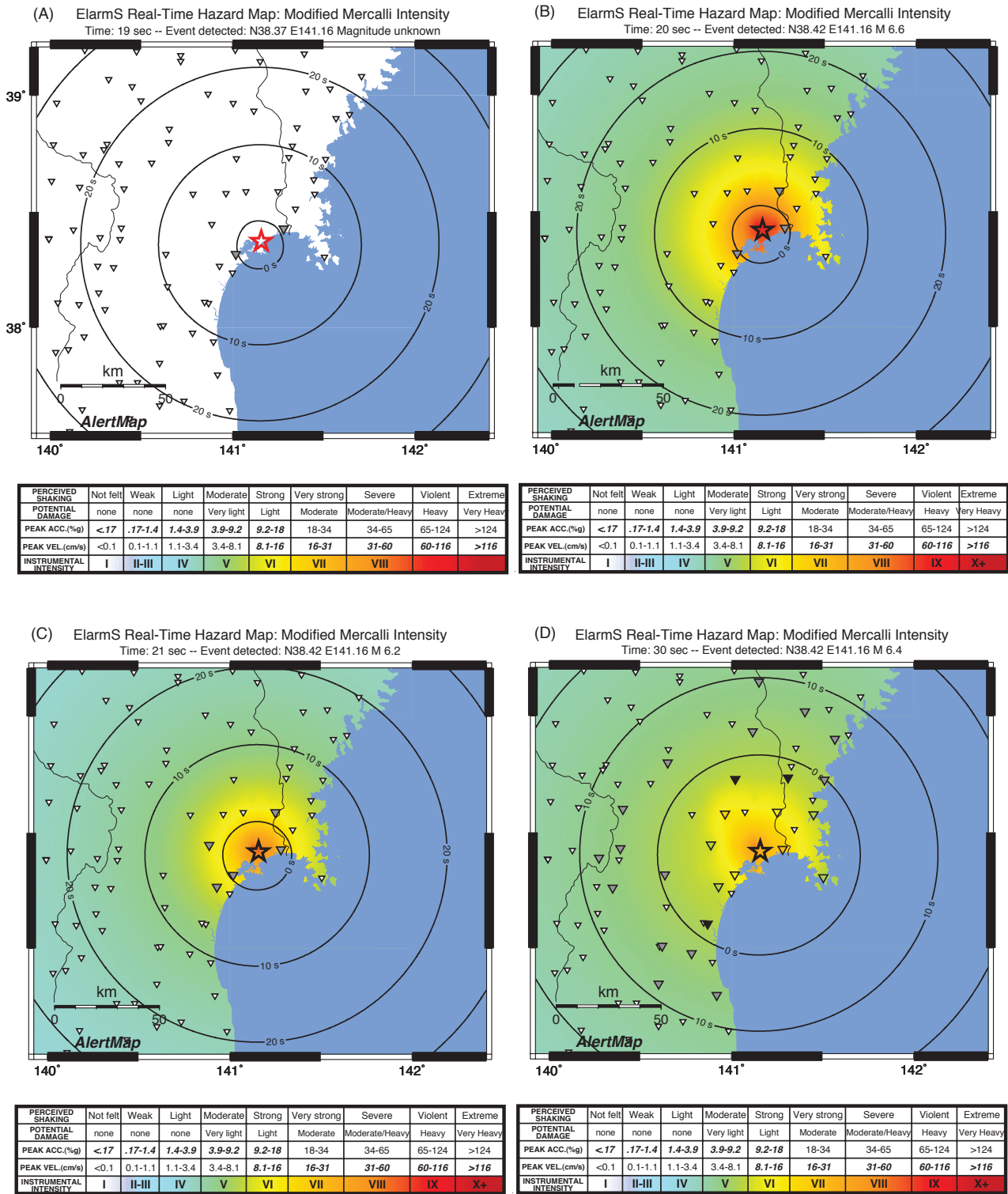
These error estimates have no units and are the natural logarithm of the ratio of the ideal PGA estimate to the ElarmS estimate. A positive error means the predicted PGA was lower than the ideal. A factor-of-two difference between the ideal and predicted PGA results in an error of 0.7, and a factor of 10 in an error of 2.3.

Monte Carlo simulations can now be used to determine the error distribution, ε_{PGA} , for any warning scenario. These errors include contributions from the magnitude estimation, the location estimation, and the attenuation relations. Each of these factors has multiple error distributions, depending on



▲ **Figure 7.** (A) Sample histogram of error in ground acceleration estimate when five stations provide PGA observations. (B) Best-fit Gaussian distributions to the PGA errors when various numbers of stations provide PGA observations. Yellow is error in estimates made with zero observations of peak ground shaking. Red is error using one station observation of peak ground shaking. Green uses two observations, blue uses three observations, black uses four observations, and purple uses five observations.

the number of reporting stations. Thus the total error, ε_{PGA} , is a function of the number of stations contributing to the location estimate, the number of stations providing P_d and τ_p^{max} values, the number of seconds of data available at each of those stations, and the number of stations reporting peak ground-motion observations. We only consider situations where the total number of triggered stations is greater than or equal to the number of stations providing magnitude estimates, which is in turn greater than or equal to the number of stations providing peak ground-shaking estimates. We consider up to five stations reporting each of the observational parameters and generate a 1,000-run Monte Carlo simulation for each of the 1,086 combinations of station contributions.



▲ **Figure 8.** AlertMap for an example earthquake, **M 6.4**, 26 July 2003, at a depth of 11.9 km. (A) The first two triggers occur simultaneously. Event location (star) is set between the triggering stations, at a depth of 8 km. Circular contours show the warning times as a function of location. (B) One second later, the first magnitude estimate, **M 6.6**, is available and translated into ground-shaking intensity across the region. A third station triggers, and the event epicenter is located by triangulating between the three triggering stations. Depth remains set at 8 km. (C) One second later, all three stations are now contributing to the magnitude estimate, which decreases to **M 6.2**. Two more stations trigger, and the five stations' total data are used to estimate an event hypocenter at a depth of 10 km. (D) The final ElarmS AlertMap, twelve seconds after the first trigger. Magnitude is **M 6.4**. Twenty-six stations are contributing to the magnitude, location, and ground-motion estimates.

The parameters for each of the resultant distributions are kept in an internal ElarmS library, to choose from for any given scenario. For example, when ElarmS makes a prediction of impending ground motions, based on a location derived from two station trigger times, two magnitude estimates (one with two seconds of data and one with one second of data), and zero peak ground shaking observations, it reports that the expected error in the predicted shaking 100 km from the epicenter is -0.13 ± 0.45 , determined from the appropriate (pre-calculated) Monte Carlo simulation. The error distribution for this scenario is shown as the red line in Figure 9(A), along with the distributions for two other example scenarios. The green line is the PGA error distribution given three stations contributing to location, two magnitude estimates (one with three seconds of data and one with two seconds of data), and one peak ground shaking observation. The blue line is the distribution given five stations contributing to location, five magnitude estimates (four with four seconds and one with three seconds), and three peak ground-shaking observations. Table 2 lists the errors predicted by the model for the example event in the Example Earthquake section, at various distances from the hypocenter. Figure 9(B) shows the distributions from all 1,086 combinations of station contributions. The mean errors for these distributions range from -0.17 to 0.20 , with a median of 0.04 . Standard deviations range from 0.32 to 0.56 , with a median of 0.39 .

Sensitivity Analysis

We perform a sensitivity analysis on the Monte Carlo error distributions to explore the source of errors in the final ground-motion predictions. Each error distribution is generated with the input of error terms for magnitude, location, and attenuation relations. One by one we set each of these error terms equal to zero, leaving the others at their observed values and recalculating all 1,086 Monte Carlo simulations.

Figure 9(C) shows the resulting distributions if the magnitude error is zero, meaning the simulated ElarmS magnitude estimate is exactly equal to the catalog magnitude. All error is due to the location estimate and attenuation relations. The mean errors of these distributions range from -0.04 to 0.21 , with a median of 0.07 . The standard deviations range from 0.31 to 0.49 , with a median of 0.37 . The mean errors are now positive and no longer centered on zero compared to the complete error model (shown in Figure 9B). The standard deviations are 5% lower than those of the complete error model, on average, resulting from the fact that there is reduced uncertainty in the PGA estimates.

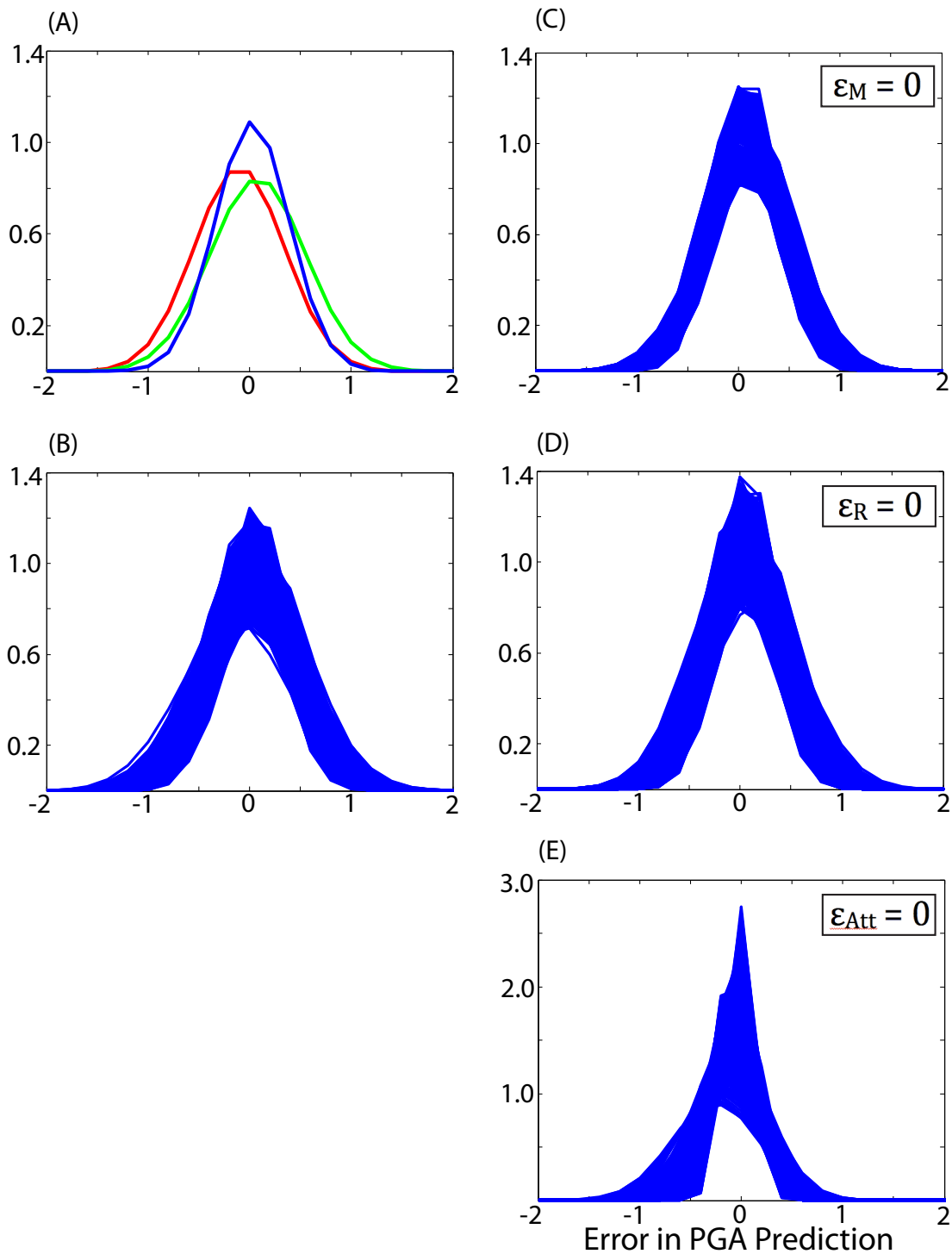
Figure 9(D) shows the distributions if the location error is zero. That is, the simulated ElarmS location estimate is exactly equal to the catalog location, and any error is due to the magnitude estimate algorithm and attenuation relations. The mean errors of these distributions range from -0.11 to 0.22 , with a median of 0.04 . The standard deviations range from 0.28 to 0.50 , with median of 0.34 . The mean errors are similar to those of the complete error model (Figure 9B), while the standard deviations are 13% lower.

Figure 9(E) shows the distributions if the error from the attenuation relation is set to zero. Here the attenuation rela-

tions are assumed to be perfect, and the only error comes from the magnitude and location estimates. The mean errors of these distributions range from -0.25 to 0.25 , with a median of -0.06 . The standard deviations range from 0.15 to 0.44 , with a median of 0.20 . This is a substantial improvement over the complete error model shown in Figure 9(B), with a mean still centered around zero but standard deviations that are 49% lower. From this we conclude that the inherent variability in ground motion at a point with respect to even the best-fitting attenuation relation is the largest source of error in the ElarmS prediction of ground shaking.

CONCLUSIONS

1. The scaling relations between P_d and magnitude and between τ_p^{\max} and magnitude are clearly evident for this Japanese dataset. This is an important result, given the large number of large ($M > 6$) earthquakes. It implies that the basic ElarmS magnitude algorithms remain robust and useful for large-magnitude events. For the entire dataset the average magnitude error and standard deviation is 0.0 ± 0.4 . For events with JMA magnitude of 6.0 or greater the error is 0.0 ± 0.5 , for $M \geq 7$ events it is -0.2 ± 0.5 . This indicates a “saturation” effect for the $M \geq 7$ earthquake, which is partly due to saturation in P -wave amplitude and partly due to difficulty in rapid and accurate locations of the large events, which are all offshore.
2. Both of the scaling algorithms, P_d and τ_p^{\max} , are independently effective at estimating final magnitude from the first few seconds of the P wave. Combining the two working methods reduces error in the final magnitude estimate when only a small number of stations are reporting and increases the overall robustness of the system. Peak displacement is vulnerable to saturation at the highest magnitudes and initial uncertainty in event location. Maximum predominant period shows more scatter for the low-magnitude events but is less sensitive to saturation at high magnitudes and uncertainty in location. A system based on both P_d and τ_p^{\max} is therefore more robust for all events.
3. While ElarmS estimated the location of the majority of events within 18 km, it struggled to accurately locate events that were far offshore. The addition of a new algorithm for determining hypocentral depth improved the location estimates of deep events, but accurate location of deep, distant events remains a challenge. The errors from these poor location estimates affect the final ground-motion predictions in this region. They also contribute to errors in the magnitude estimate made from peak displacement observations, since these are scaled by epicentral distance. We note that for current real-time processing in California, these location difficulties are not pertinent, as most events are on- or near-shore, and nearly all are shallower than 20 km (Hill *et al.* 1990).
4. A new error model for ElarmS provides a library of error distributions generated by Monte Carlo simulations. Every ElarmS prediction of magnitude, location, and ground



▲ **Figure 9.** Results from the Monte Carlo simulation of the ElarmS error model. (A) Three examples showing best-fit Gaussian distributions for errors in ground-motion estimation given various quantities of data input. The red line is the error if two stations contribute to a location estimate, two stations contribute to the magnitude estimate (one using one second of *P*-wave data, one using two seconds), and zero stations report PGA observations. The green line is the error if three stations contribute to the location estimate, two stations contribute to the magnitude estimate (one with two seconds of *P*-wave data, one with three seconds), and one station reports a PGA observation. The blue line is the error if five stations contribute to the location estimate, five stations contribute to the magnitude estimate (four with four seconds of *P*-wave data, one with three seconds), and three stations report PGA observations. (B) All 1,086 error distributions resulting from the error model. Each line represents a unique combination of data inputs. (Figures C–E) show the sensitivity analysis: (C) Error model if magnitude estimate contains no error. (D) Error model if location estimate contains no error. (E) Error model if ground motion estimate contains no error.

TABLE 2
PGA Errors for Example Event, 26 July, 2003

	(b) 1 second	(c) 2 seconds	(d) 12 seconds
Mean Observed Error	0.05 ± 0.25	-0.05 ± 0.25	0.13 ± 0.26
Predicted Error, 20km	-0.09 ± 1.38	-0.20 ± 1.36	-0.18 ± 1.37
Predicted Error, 50km	-0.13 ± 0.77	-0.11 ± 0.56	-0.11 ± 0.64
Predicted Error, 100km	-0.01 ± 0.39	-0.02 ± 0.38	0.01 ± 0.37

motions can now be provided with an associated uncertainty, based on the quantity of data contributing to the prediction. Uncertainty estimates are essential for both internal study of the system and for potential end users, who must decide whether to act on a given prediction. Using Monte Carlo simulations we explore the full range of errors in PGA predictions from the first estimate using one second of *P*-wave data at the first station to trigger to using *P*-wave data and PGA observations at five stations. The error distributions have mean errors of -0.2 to 0.2 (median 0.0) and standard deviations of 0.3 to 0.6 (median 0.4). A factor-of-two error in the predicted PGA relative to the observed PGA corresponds to an error of 0.7.

5. We find that the most significant contribution to the error in ElarmS' final ground-motion prediction comes from the inherent variability in peak ground motion at a given location with respect to even the best-fitting attenuation relations. Calculating regional ground motions from attenuation relations using only the estimated magnitude and location of the earthquake resulted in less error than did the same calculation with the addition of the first one or two observations of peak ground motion. Only when three or more station observations are combined does their inclusion in ground shaking estimation improve the accuracy of the predictions.

The continued improvement of the ElarmS methodology increases its utility in California and in other regions. An accurate, prompt, and reliable early warning system in any seismic setting has the potential to reduce loss of life and money during a damaging earthquake. The developments from this study bring ElarmS one step closer to providing reliable real-time warnings to the public. ☒

ACKNOWLEDGMENTS

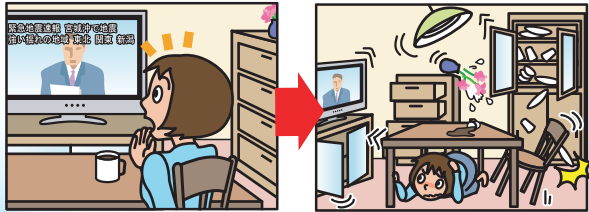
We thank K-NET for the use of their data. Research supported by the U.S. Geological Survey (USGS), Department of the Interior, under USGS award number 06HQAG0147. The views and conclusions contained in this document are those of the authors and should not be interpreted as necessarily representing the official policies, either expressed or implied, of the U.S. Government. This is Berkeley Seismological Laboratory contribution number 09-17.

REFERENCES

- Allen, R. M. (2004). Rapid magnitude determination for earthquake early warning. In *The Many Facets of Seismic Risk*, ed. G. Manfredi *et al.*, 15–24. Naples, Italy: Università degli Studi di Napoli “Federico II.”
- Allen, R. M. (2006). Probabilistic warning times for earthquake ground shaking in the San Francisco Bay area. *Seismological Research Letters* **77** (3), 371–376.
- Allen, R. M. (2007). The ElarmS earthquake early warning methodology and application across California. In *Earthquake Early Warning*, ed. P. Gasparini, G. Manfredi, and J. Zschau, 21–44. Milan, Italy: Springer Ital.
- Allen, R. M., and H. Kanamori (2003). The potential for earthquake early warning in southern California. *Science* **300**, 786–789.
- Allen, R. M., H. Brown, M. Hellweg, O. Khainovski, P. Lombard, and D. Neuhauser (2009). Real-time earthquake detection and hazard assessment by ElarmS across California. *Geophysical Research Letters* **36**, L00B08
- Boore, D. M., W. B. Joyner, and T. E. Fumal (1997). Equations for estimating horizontal response spectra and peak accelerations from western North American earthquakes: A summary of recent work. *Seismological Research Letters* **68** (1), 128–153.
- Hill, D. P., J. P. Eaton, and L. M. Jones (1990). Seismicity, 1980–86. In *The San Andreas Fault System, California*, ed. R. E. Wallace, 115–152. USGS Professional Paper 1515.
- Lockman, A. B., and R. M. Allen (2005). Single-station earthquake characterization for early warning. *Bulletin of the Seismological Society of America* **95**(6), 2,029–2,039.
- Olson, E. L., and R. M. Allen (2005). The deterministic nature of earthquake rupture. *Nature* **438**, 212–215.
- Tsang, L., R. M. Allen, and G. Wurman (2007). Magnitude scaling relations from *P*-waves in southern California. *Geophysical Research Letters* **34** L19304.
- Wald, D. J., B. C. Worden, V. Quitoriano, and K. L. Pankow (2005). *ShakeMap Manual: Technical Manual, Users Guide, and Software Guide*; <http://pubs.usgs.gov/tm/2005/12A01/pdf/508TM12-A1.pdf>.
- Wurman, G., R. M. Allen, and P. Lombard (2007). Toward Earthquake Early Warning in Northern California. *Journal of Geophysical Research* **112**, B08311.
- Youngs, R. R., S.-J. Chiou, W. J. Silva, and J. R. Humphrey (1997). Strong ground-motion relationships for subduction zones. *Seismological Research Letters* **68** (1), 58–73.
- Zollo, A., M. Lancieri, and S. Nielsen (2006). Earthquake magnitude estimation from peak amplitudes of very early seismic signals on strong motion records. *Geophysical Research Letters*. **33**, L23312.

Seismological Laboratory
University of California, Berkeley
215 McCone Hall # 4760
Berkeley, California A 94720-4760 U.S.A.
hollybrown@berkeley.edu
(H. B.)

- 家庭では
- ・頭を保護し丈夫な机の下などに隠れる
 - ・あわてて外へ飛び出さない
 - ・無理して火を消そうとしない



人がおおぜいいる施設では

- ・係員の指示に従う
- ・落ちついて行動
- ・あわてて出口に走り出さない



緊急地震速報「利用の心得」

自動車運転中は

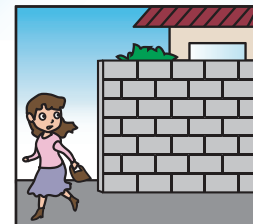
- ・あわててスピードをおとさない
- ・ハザードランプを点灯し、まわりの車に注意を促す
- ・急ブレーキはかけず、緩やかに速度をおとす
- ・大きな揺れを感じたら、道路の左側に停止



周囲の状況に応じて
あわてずに
まず身の安全を確保する！

緊急地震速報は見聞きしてから、強い揺れが来るまでの時間が数秒から数十秒しかありません
その短い間に身を守るための行動を取る必要があります

屋外(街)では



- ・ブロック塀の倒壊等にご注意
- ・看板や割れたガラスの落下にご注意
- ・丈夫なビルのそばであればビルの中に避難

鉄道・バス乗車中は

- ・つり革、手すりにしっかりつかまる



エレベーターでは

- ・最寄りの階で停止させすぐに降りる



山やがけ付近では

- ・落石やがけ崩れにご注意

